CHAPTER 2

Operational Tools

Introduction

In the field of grain boundary engineering the main objective is to manage an increase in relatively special grain boundaries. Therefore a technique that monitors both microstructural and orientation information is of vital importance. This may not only yield grain boundary information, but also grain size distributions as well as preferred orientations can then be observed.

In this chapter, an attempt is made to familiarise the reader with a relatively new technique, which is called Electron Backscatter Diffraction (EBSD). This technique is nowadays used in correlation with software incorporating fully automated procedures for recognizing and indexing Kikuchi bands. This reconstruction technique is called Orientation Imaging Microscopy (OIM).

In addition, transmission electron microscopy (TEM) is being discussed. It enables a more detailed and more local observation of microstructure and orientation. Furthermore, representations of preferred orientations like pole figures and orientation distribution functions (ODF's) will be highlighted.

2.1 Hardware of the OIM

The EBSD equipment is attached to a Philips XL30-S FEG Scanning Electron Microscope (SEM). Therefore, first, an introduction of the SEM technique will be given and subsequently the EBSD hardware will be addressed.

2.1.1 Scanning electron microscopy

Electron microscopy is often used to study microstructural as well as morphological features of engineered materials [1]. In scanning electron microscopy (SEM) an electron beam is focused and scanned across a surface. When the electrons hit the specimen, a variety of signals is generated due to the interaction of a primary electron with matter. Every signal recorded by one of the detectors gives specific information of the sampled volume of the specimen or its chemical content.

A schematic figure of a scanning electron microscope is presented in Fig. 2.1. In a Philips XL-30 S FEG-SEM, electrons are generated by the field emission (electron) gun using a high electrostatic field. Then the electrons are accelerated with an energy between 1 keV and 30 keV down the column towards the specimen. The magnetic lenses (condensor lens and objective lenses) focus the beam to a spot with a diameter of approximately 1-10 nm on the specimen. The electron beam is swept over the surface of the sample by the scanning coils. The magnified image is formed by relating the detector signal to the position of the beam.

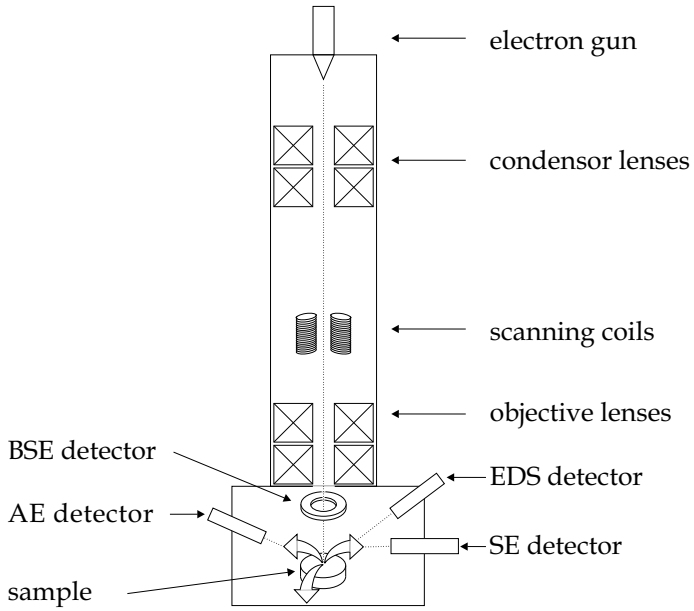

Fig. 2.1: Schematic picture of the scanning electron microscope.

Secondary electrons, used for imaging, are produced when loosely bound atomic electrons in this solid are released by the interaction with a primary

electron. These secondary electrons have a small mean free path because of the low energy they have. Therefore, the information is extracted from a shallow depth (~10 nm) [2].

2.1.2 EBSD Hardware

The EBSD technique relies on positioning the specimen within the SEM chamber such that a small angle, typically 20°, is made between the incident electron beam and the specimen surface. This enhances the fraction of backscattered electrons able to experience diffraction by lattice planes in the sampled volume and to escape from the specimen surface. The resulting electron diffraction pattern (EBSP), also known as Kikuchi pattern, can be captured by a fluorescent screen (Fig. 2.2) [3].

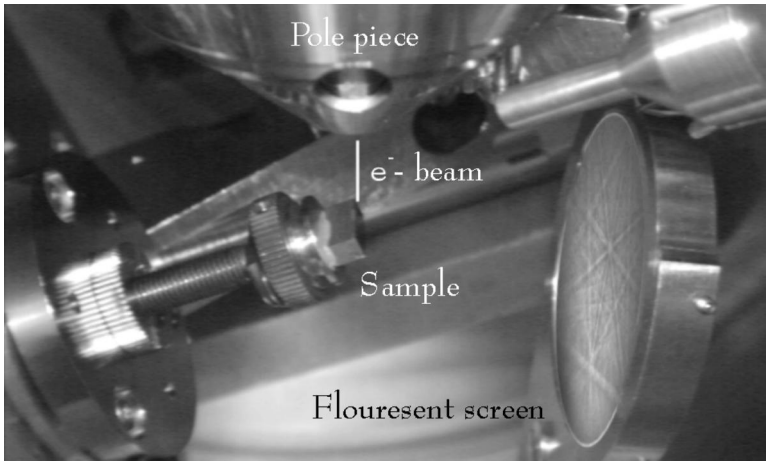

Fig. 2.2: Configuration in the microscope chamber for EBSD operation.

One of the most important components of the OIM system is the camera obtaining diffraction images [4]. The capability of the camera system in obtaining images with low brightness in a short time lapse will dictate the SEM operating conditions required. The camera control unit (CCU), the Hamamatsu C2400, receives the signal from the camera and provides a television output video signal. The CCU generally has controls for electronically altering the intensity gradient across the detector so that the raw image is as smooth as possible. Gain control and black level are also typically included for user manipulation of the raw images. The output signal is sent to an image-processing unit. The image processor enhances the signal and corrects for any intensity gradients across the phosphor screen. This is done by first collecting a signal from a large part of the material being analysed. Averaging should be

performed to remove some noise in the system. Thereafter, the EBSP collected from the large area is stored in a buffer. Each time an EBSP is captured, this buffer is automatically subtracted from the EBSP, which result an enhanced contrast level. The processed signal simultaneously with the optional EDS data is sent to the computer for analysis by way of the MSC-1100.

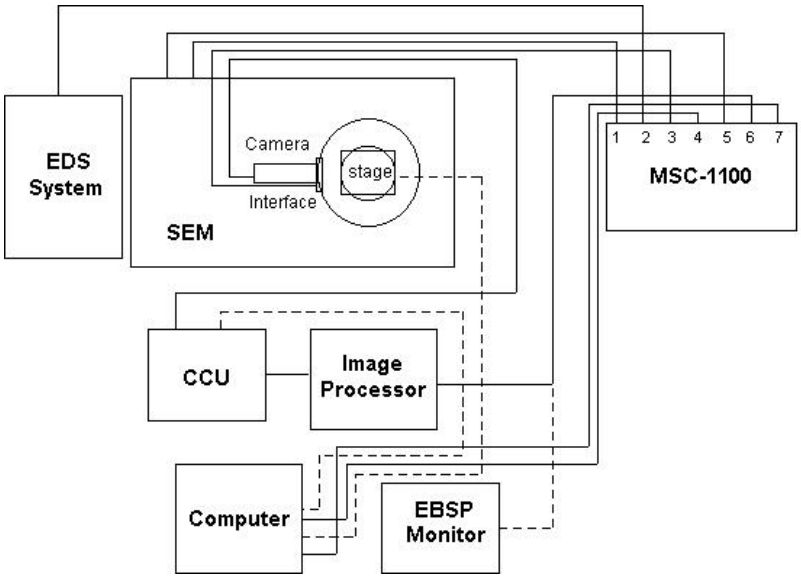

Fig. 2.3: Schematic picture of the EBSD Hardware.

2.2 Formation and analyses of electron backscattered patterns

The formation, capturing and subsequent indexing of the Kikuchi patterns are the basic mechanisms which are inevitable for electron backscatter diffraction. This section describes these processes.

2.2.1 Formation of an EBSP

The angles θ at which diffraction occurs depend on both the wavelength λ and the interplanar spacing d of the planes on, which scattering occurs. The specific angle at which reflection is observed is termed the Bragg angle θ_B. For most crystal structures, reflection through the respective Bragg angle is not observed for all possible sets of lattice planes. In general, the relative intensity of a given reflector and, consequently, the rules of extinction, can be deduced from calculating the so-called structure factor [5].

As the primary electrons enter a crystalline solid, they are diffusely and inelastically scattered in all directions. These scattered electrons may impinge on crystal planes at the Bragg angle. Since diffraction of the elastically scattered electrons through the Bragg angle is occurring in all directions, the result is a cone which extends about the normal of the reflecting atomic planes with half apex angle 90°- θ_B. Each family of planes gives rise to two cones, one from either side of the imaginary source (Fig. 2.4). The Bragg angle, for typical values of the electron wavelength and lattice interplanar spacing, is found to be about 0.5°. Consequently, the apex angle of a diffraction cone is close to 180°, i.e. the cones are almost flat. When the phosphor screen intercepts the diffractions cones, a pair of parallel conic sections results, which appear to be parallel lines. These are called Kikuchi lines.

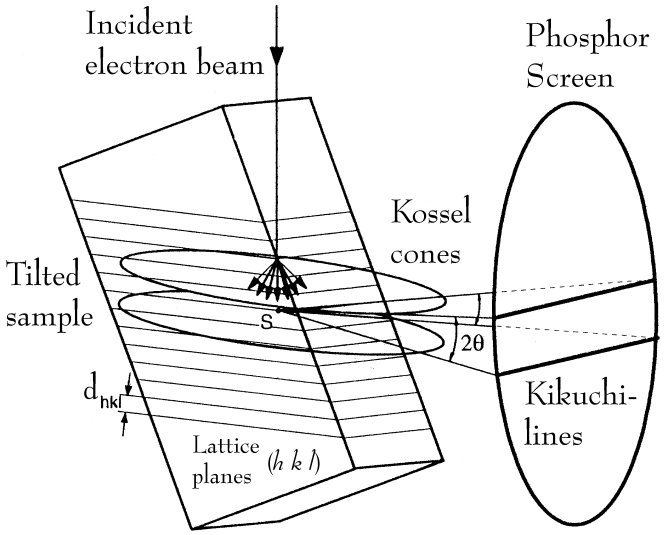

Fig. 2.4: Inelastic scattered electrons from specimen generating Kikuchi-lines on fluorescent screen.

The whole EBSD Kikuchi pattern consists of pairs of parallel lines where each pair is known as a Kikuchi band. It has a distinct width and corresponds to a distinct crystallographic plane. The intersection of bands corresponds to a zone axis (pole). The Kikuchi pattern therefore essentially embodies all the angular relationships in a crystal, both the interzonal and interplanar angles are present, and therefore implicitly contain the crystal symmetry. The EBSD Kikuchi pattern is therefore a gnomonic projection onto a flat surface [6].

2.2.2 Analyses of an EBSP

Commercial automated systems attempt to determine the orientation based on the geometrical arrangement of bands in the EBSP or Kikuchi pattern. Therefore, the first step in automated indexing of EBSPs is to extract the bands from the pattern. Krieger Lassen et al. [7] first suggested using the Hough transform to extract band information [8]. This has proven to be in general a robust method and is therefore most commonly employed today.

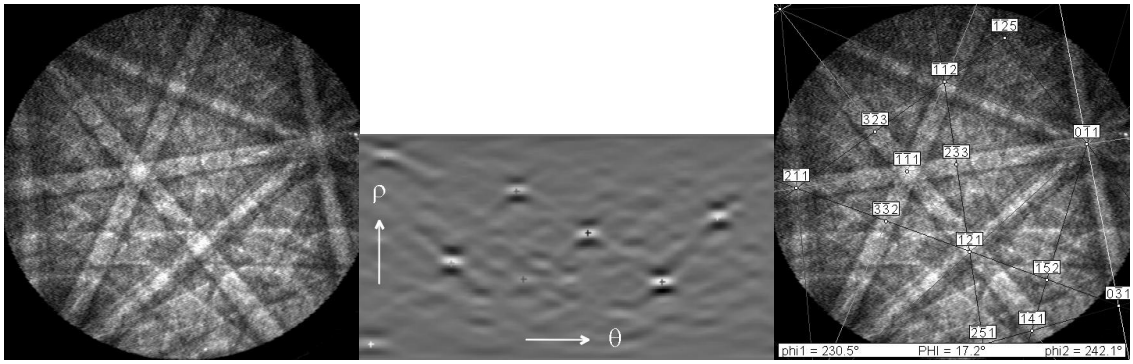

Fig. 2.5: A Kikuchi pattern *(left)* is transformed to Hough space *(middle)* where single high intensity peaks are detected, after band/ point detection an orientation can be determined using this configuration of the bands *(right).*

The equation governing the Hough transform is

$$\rho = x\cos\theta + y\sin\theta$$

Where (x , y) describe a set of pixel coordinates forming a line and the Hough parameters (ρ , θ) provide a wave like function in Hough space. As the intensity of each (x , y) pixel is added, the problem of finding a Kikuchi band is now reduced in finding a peak of relatively high intensity in the Hough transform (Fig. 2.5 *middle*). Where the specific "butterfly" contrast profile in the ρ direction of the Hough peak may function as an additional recognition feature.

Once the bands have been detected, the reflecting planes associated with the detected bands must be identified. Two band characteristics can be used for indexing; (1) the width of a band, which is a direct function of the d-spacing through Bragg's law, this option is a powerful tool for improved accuracy dealing with structures of low symmetry and for phase identification. (2) The angles between the (located) bands which are known and compared to a

theoretical directory of interplanar angles; this is the standard method used in our TSL software.

Selection of the most likely indexing solution for automated systems is to use a voting scheme. Each time the angles in a triplet of bands are compared to the look-up table allowing the Miler indices *(h k l)* associated with the bands to be identified. All possible solutions within the tolerance angle are registered for any triplet and each solution yields a vote. The most probable solution is the one that receives the majority of votes.

In order to assess the reliability of the indexing, several parameters such as the *image quality* (IQ), the *confidence index* (CI) and the *fit* between the recalculated and the detected bands may be discerned. The IQ reviews the relative quality of the pattern using the intensities of the found Hough peaks. The CI is given by

$$CI = \frac{(V_1 - V_2)}{V_{total}}$$

Where V_1 and V_2 are the number of votes for the first and second solutions and V_{total} represents the total possible number of votes from the detected bands. The CI will yield a value between 0 and 1. The comparison between the two highest numbers of votes gives this quantity a doubtful character and may be misleading. Especially in the case where V_1 equals V_2, this results a CI of 0. The pattern however may be properly indexed. In general, CI values higher then 0.2 will represent a proper indexed pattern [9]. The *fit* parameter defines the average angular deviation between the recalculated and the detected bands. It is often simply a measure of how well the system is calibrated and the parameters defining the crystal structure are defined.

2.3 Orientations and misorientations

To specify an orientation, it is necessary to define a reference frame consisting of at least two axes, which is known as a coordinate system. Important surfaces or directions associated with the shape of the specimen are commonly used to define the axes. The direction normal to the specimen surface is called 'surface normal' (SN), in-plane directions are the 'rolling direction' (RD) and 'transverse direction' (TD).

The crystal coordinate system is specified by directions in the crystal. In the case of orthogonal symmetry (includes cubic symmetry) the axes [100], [010]

and [001] already form an orthogonal frame. Therefore, these axes are used as the crystal coordinate system.

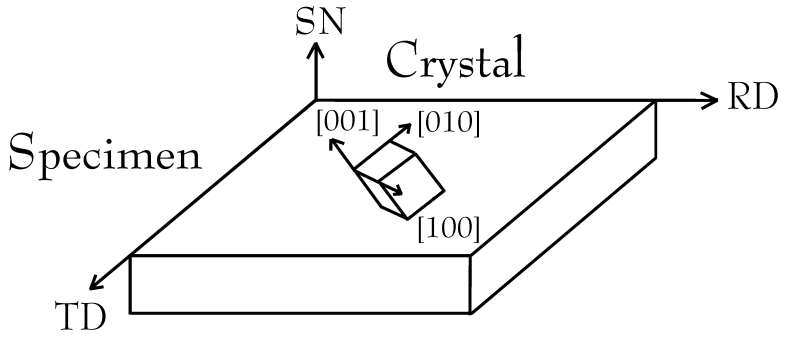

Fig. 2.6: Coordinate systems of specimen and orthogonal symmetric crystal.

The orientation of a crystal can now be specified relatively to the specimen coordinate system by

$$\vec{M}_C = g \,.\, \vec{M}_S$$

Where $\vec{M}_C$ and $\vec{M}_S$ are the unit vectors of the crystal and specimen systems, g is the rotation matrix. Orientations can be represented by the rotation matrix or by using Euler angles. All the notations can be converted from the rotation matrix. The description of an orientation is user dependent but unambiguously fixed with respect to its reference frame.

As the coordinate system is changed from the specimen to an other crystal (with the same crystal structure) coordinate system, the misorientation between two crystals can be obtained by

$$g_m = \vec{M}_{C1} \,.\, \vec{M}_{C2}^{-1}$$

Where $\vec{M}_{C1}$ and $\vec{M}_{C2}$ refer to the two crystal coordinate systems, g_m is the misorientation matrix. The misorientation is normally addressed as an angle (θ) / axis (<*h k l*>) pair

$$\theta = cos^{-1}\left(\frac{Tr[g_m]-1}{2}\right) and$$

$$h = g_{m32} - g_{m23}, k = g_{m13} - g_{m31}, l = g_{m21} - g_{m12}$$

Orientations are presented in our case by Euler angles or as a (hkl)[uvw] pair. Visualizing orientations can be a convenient tool, which is used in a discrete way or as an intensity plot. Representations can appear in several forms; the orientation distribution function (ODF) and pole figures are most commonly used. Therefore, these representations will be highlighted in the next sections.

2.3.1 Pole Figures

Stereographic projections plot the normal of crystallographic planes onto great circles, which serve as the representation of the pole (Fig. 2.7). The intersection of crystallographic poles with the surface of the sphere is the basis of the stereographic projection method. The line, containing the intersection of the sphere's surface and the south pole of the sphere, intersects the equatorial plane.

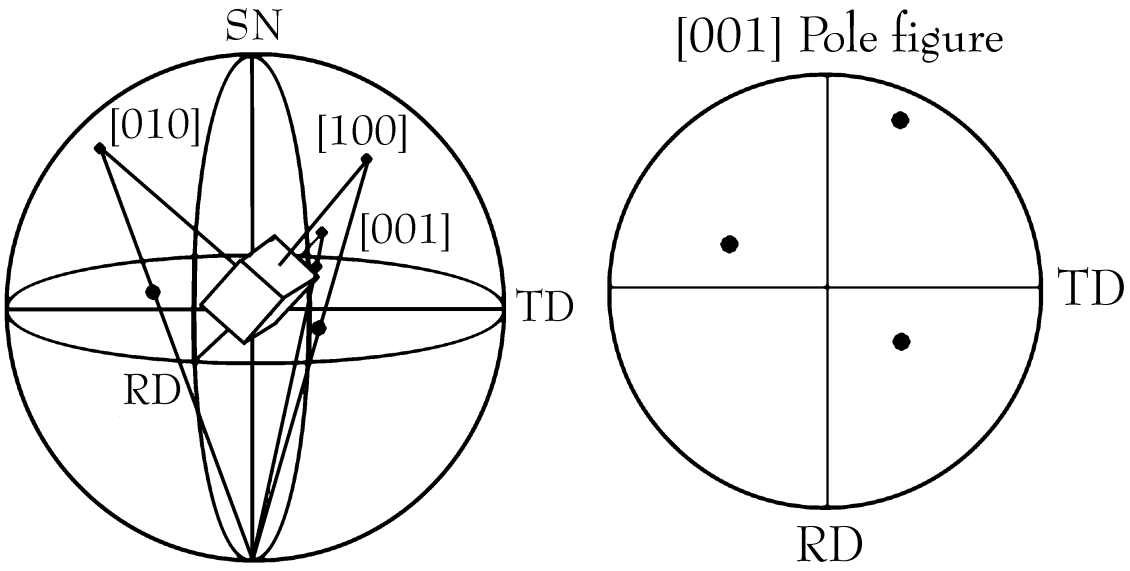

Fig. 2.7: Formation of a standard [001] pole figure *(left)*; projections of intersections with the surface of the sphere to South Pole onto RD-TD plane *(right)* forms a 2D representation of a 3D orientation.

This yields a two dimensional projection. When all zones are included, it directly maps out the angular relationships between projected normals, which are related to the crystal structure. This visualisation technique is also known as a pole figure.

2.3.2. Orientation Distribution Function (ODF) in Euler space

As already, mentioned, an orientation can be presented in several ways; the ODF uses Euler angles for representation. The complete orientation of a crystal must be specified by at least three Euler angles, which are defined as follows (Fig. 2.8); if the crystal frame of reference is aligned to the specimen coordinate system, the first angle, φ_1, rotates around the [001] z axis, the second angle, ϕ, about the new [100] x axis and the third angle, φ_2, about the new [001] z axis.

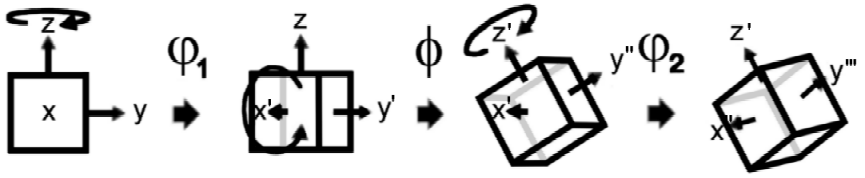

Fig. 2.8: Definition of the Euler angles in a cubic system.

The Euler angles essentially describe the orientation of a crystal rather than the plane as in the case of a pole figure, and hence require a three dimensional representation (Fig. 2.9). Usually, the angular parameters are plotted as Cartesian coordinates and the density function (describing the frequency of crystals having a specific orientation) is projected parallel to φ_2. The density function is a powerful tool to subtract preferred orientations, i.e. texture, from intensity differences in the ODF. The intensity is calculated as the ratio of the observed density over the random density (for a random distribution of grains) and is therefore given as times-random values.

Due to specific processing conditions and slip system configurations, typical texture components may exist for different crystal structures [10]. The intensity of the components present describes the anisotropy of the material. The typical texture components occurring in Aluminium (Face Centred Cubic) (Fig. 2.10) and Ferrite (Body Centred Cubic) are given in table 2.1 [11,12]. The H, I, Brass and Goss components belong to the so-called α-fibre texture, whereas the F, E, Brass, Copper and S components belong to the γ-fibre.

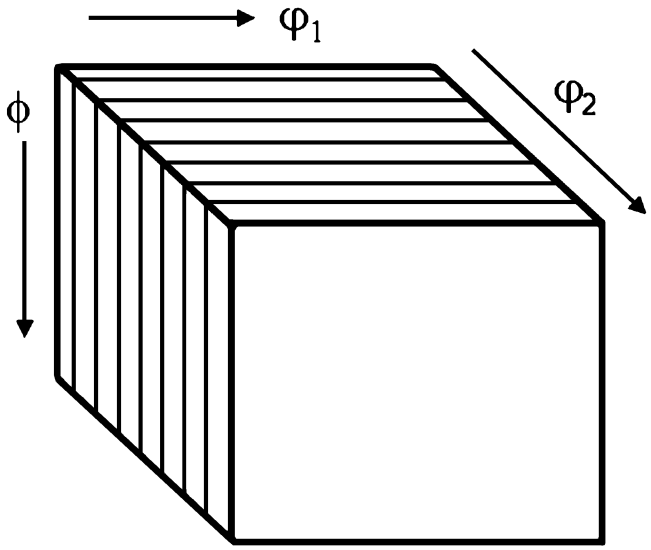

Fig. 2.9: Binned Euler space with the density function parallel to φ_2.

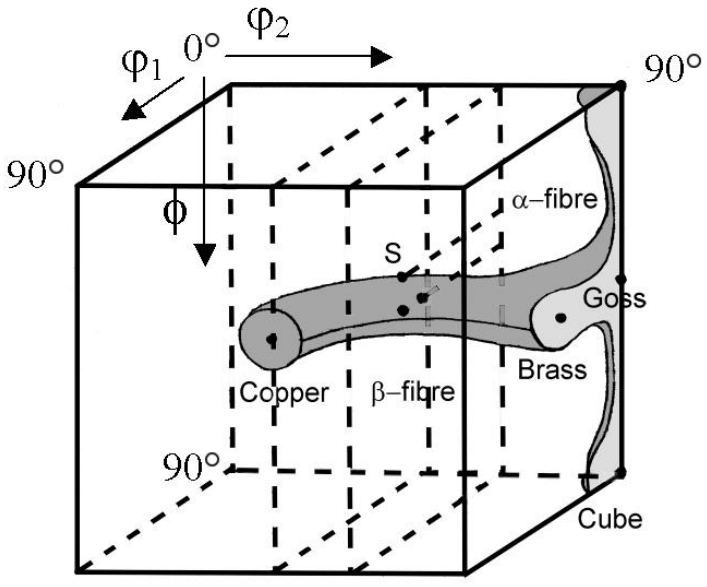

Fig. 2.10: Typical texture components in Al appointed in a schematic ODF.

Table 2.1: Typical texture components existing in α-Fe and Al.

Ferrite components	{hkl}<uvw>	Euler angles (φ_1, ϕ, φ_2)	Aluminium components	{hkl}<uvw>	Euler angles (φ_1, ϕ, φ_2)
H	{001}<110>	(0°, 0°, 45°)	Cube	{001}<100>	(0°, 0°, 0°)
I	{112}<110>	(0°, 25°, 45°)	Goss	{011}<100>	(0°, 45°, 0°)
E	{111}<110>	(0°, 54.7°, 45°)	Brass	{011}<112>	(35°, 45°, 0°)
F	{111}<112>	(30°, 54.7°, 45°)	Copper	{112}<111>	(90°, 35°, 45°)
			S	{123}<412>	(47°, 37°, 63°)

The occurrence of those orientations, especially at high intensities, might introduce some preferred next neighbour misorientations. In the case of one strong texture component a high amount of low angle grain boundaries is expected. As a fibre texture (only one crystal axis is fixed) occurs, a preferred misorientation axis will be present. As a result, grain boundary engineering is a possibility. Especially so-called 'special' or low Coincidence Site Lattice (CSL) grain boundaries are preferred.

2.3.3. Coincidence Site Lattice Boundaries

It has been observed that phenomena associated with grain boundaries (e.g. corrosion, segregation etc.) are influenced by the grain boundary characteristics [13]. The occurrence of such phenomena has been often linked to particular boundary geometries. Boundaries that have markedly different values for these properties than an average boundary were called 'special' or CSL boundaries. A special boundary is beneficial because it shows higher resistance to intergranular degradation.

These CSL boundaries are classified in terms of Σ values. The Σ value denotes the fraction of atoms in coincidence if two neighbouring crystals virtually will overlap, e.g. a Σ5 boundary has 1 on 5 atoms at coincident sites (Fig. 2.11). The Σ classification of a grain boundary is therefore only determined by the misorientation. If all five degrees of freedom, which are necessary for a proper classification of the grain boundary, would be resolved, the translation of the crystals i.e. the grain boundary plane is obtained. Because the OIM data is

collected on the specimen's surface, only a trace of the boundary can be observed. Thus, serial sectioning or other stereological approaches are needed to extract the complete boundary normal information.

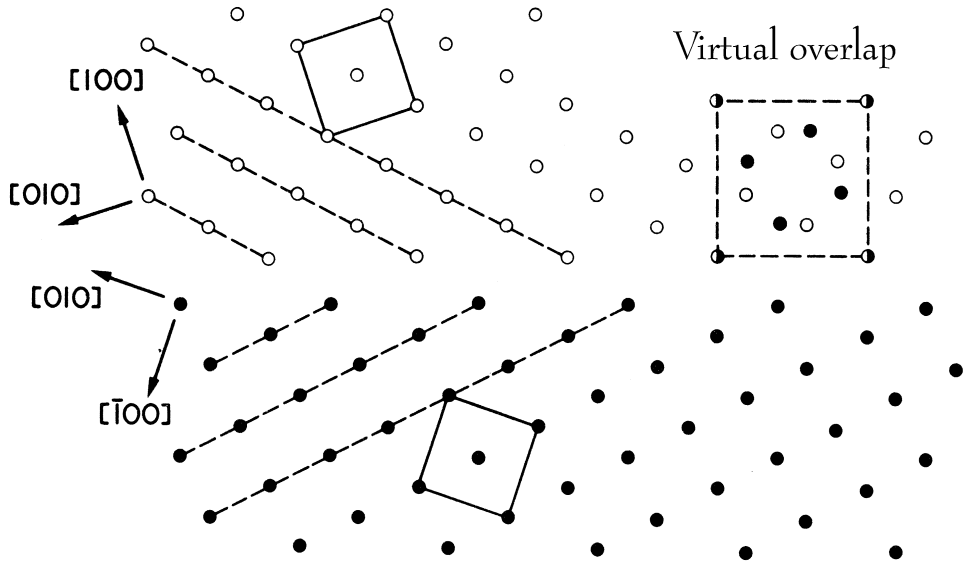

Fig. 2.11: Schematic representation of Σ5 boundary, 1 on 5 atoms overlap.

Special boundaries retain their ordered, relatively low energy, structures at misorientations deviating from those giving geometric matching. A criterion for the maximum allowable deviation at which a boundary remains special must be adopted and is given by

$$\Delta\theta = \frac{15^0}{\Sigma^n}$$

Where Δθ represents the maximum allowable angle, Σ is the grain boundary classification and n varies between 0.5 and 1. The standard criterion is known as Brandon's criterion and holds for n = 0.5 [14].

2.3.4. Orientation Imaging Mapping

The EBSD technique is nowadays fully automated. During operation in the SEM, the beam scans the sample surface or the stage moves underneath the beam in a hexagonal grid. At each pixel, an EBSP is captured and analysed, the data obtained is stored on disk. Finally, the software corrects for the sample tilt of 70° and reconstructs the obtained data to the x and modified y coordinates [15]. This allows the user to relate orientations to the corresponding (micro) structure. This is called the Orientation Imaging Microscopy (OIM) technique.

In order to accurately obtain the orientation from the indexing of a diffraction pattern during scanning, three calibration constants x, y and *l* are necessary to derive. This indicates the sample position with respect to the electron beam and the fluorescent screen, as shown in the schematic image below (Fig. 2.12).

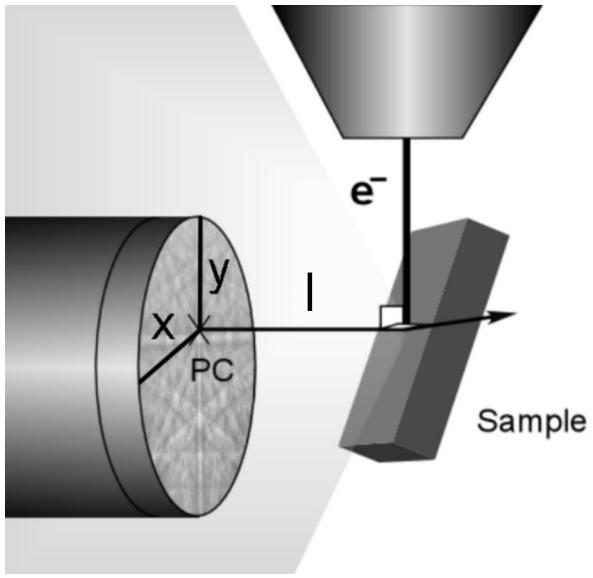

Fig. 2.12: Schematic of the geometry including calibration parameters.

The parameter *l* is defined as the distance from the intersection of the electron beam with the sample to the phosphor screen. This parameter is adjusted when the position of the fluorescent screen is altered. The coordinates x and y arise from the intersection of a vector originating at the intersection of the electrons with the sample with a direction normal to the electron beam on the phosphor screen. This is often referred to as the "Pattern Centre".

The pattern centre is altered as the beam changes its position on the sample surface. This has a large impact as large areas have to be scanned (> 2 mm^2). Therefore, a shift from beam-controlled scanning to stage-controlled scanning should take place when a large scan is initiated. The disadvantage of stage-scanning is that the scanning time is increased by a factor of 10, due to the movement of the stage. Therefore, stage-scanning was only applied in the case of a texture scan on aluminium, due to its large grain size.

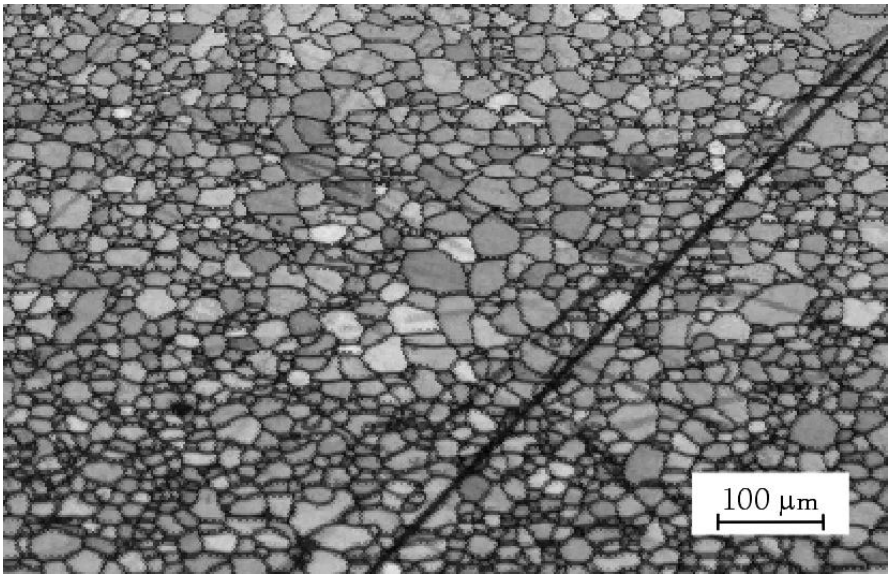

Fig. 2.13: IQ map showing grain structure of ULC steel including surface scratches.

To reveal whether the scan is correctly performed, or whether the sample surface is free of contaminations or scratches, an IQ map is plotted. The image shows many similarities to a normal secondary electron image, for example in Fig. 2.13 grain boundaries and some scratches can be clearly seen (IQ is low). At sites of low IQ, the indexing may not be properly carried out. Therefore, these pixels should be treated with care. An algorithm can be used to substitute them.

The orientation and misorientation data can easily be visualised in two or more so-called inverse pole figure (IPF) maps. A single orientation cannot be visualised by a single map because a map shows only one direction with respect to a sample axis, instead of two directions, which constructs an orientation (Fig. 3.15, 17 and 18, page 43-44). A distinct misorientation, for instance a special boundary (CSL boundary), may be highlighted by a certain user defined colour. This holds also for angles and axis.

2.4 Transmission Electron Microscopy

Transmission electron microscopy (TEM) provides also data on structure, phase and crystallography yet at a local scale, down to atomistic levels. This enables a detailed study on the morphology and deformed state of matter.

2.4.1 Configuration of a TEM

The present research is done with the use of an analytical JEOL 2010F TEM. The schematic representation of a TEM is depicted in Fig 2.14. Again, the electrons are generated by the field emission (electron) gun using a high electrostatic field. This results in a high source brightness and a coherent beam with a small energy spread. These conditions are ideally suited for analytical or high-resolution purposes.

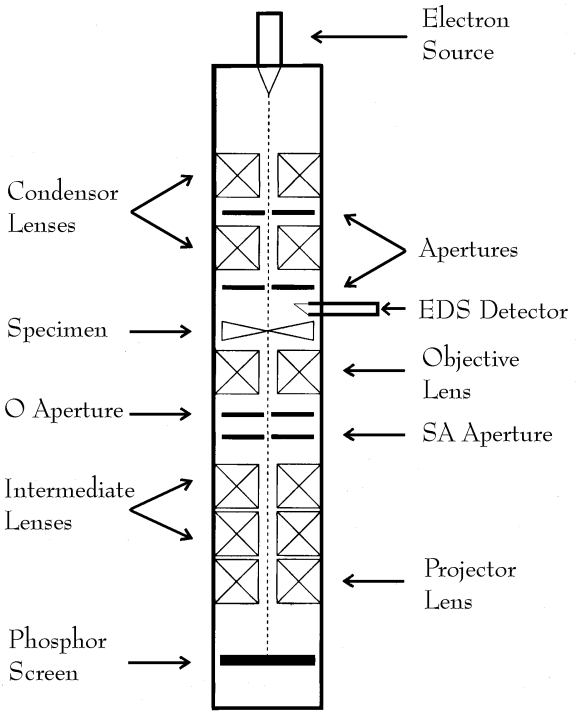

Fig. 2.14: Schematic overview of a transmission electron microscope.

The electrons are accelerated up to 200 keV. The electron beam is correctly aligned as it travels parallel to the optical axis and is respectively focused. Subsequently, a relatively thin specimen will be hit by the electrons introducing numerous interactions. Each scattering event produces its own unique signal, which can be recorded. Every signal recorded by one of the detectors gives specific information of the sampled volume of the specimen.

2.4.2 Visualization of micro- and crystal structure in TEM

An image in TEM is mainly formed by elastically scattered electrons. These scattered electrons result in scattered beams that are, together with the undiffracted beam, projected on the fluorescent screen. The image contrast can easily be enhanced by using only the transmitted beam and blocking the scattered beams making use of the objective aperture. The main factor causing the high spatial resolution is the small wavelength of the used electrons. However, the resolution is limited by the relatively poor performance of the electromagnetic lens systems, particularly by the spherical aberration C_s.

As in the OIM configuration, the elastically scattered electrons can be used to obtain information on the crystallography of the sample. As a function of sample thickness two different approaches can be used, spot and Kikuchi diffraction (Fig. 2.15). In the case of a relatively thin area, spot diffraction can be obtained. A coherent beam will strike the specimen and diffraction is likely to occur for the geometry for which the Bragg angle (Ch. 2.2.1) is achieved. Constructive interference of the diffracted electrons will yield a diffracted beam. In the case of a relatively thick sample, the electrons, just like in an SEM sample, will now diffusively scatter and subsequently produce Kossel cones. The cones will intersect the Ewald sphere, creating parabolas, which approximate to straight Kikuchi lines in the diffraction patterns.

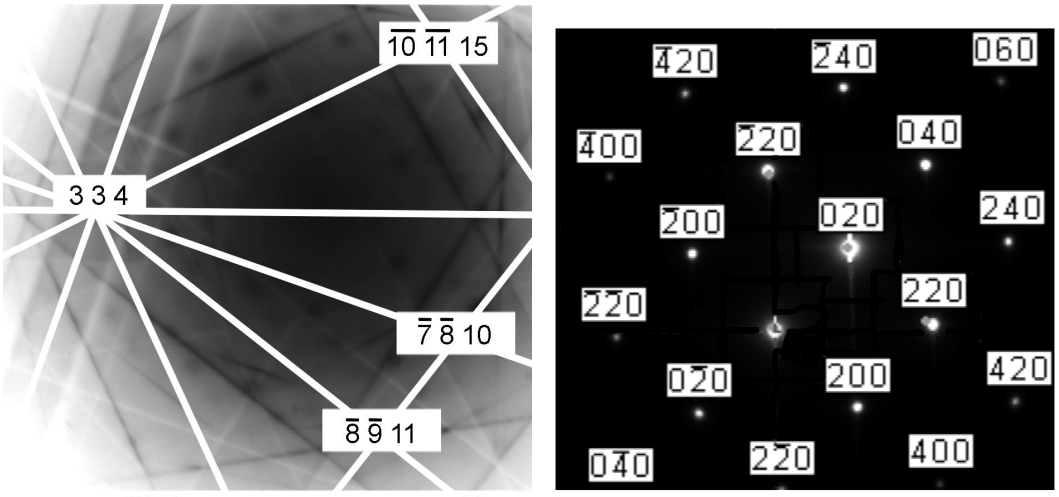

Fig. 2.15: Indexed Kikuchi pattern and spot pattern making use of ACT 300.

The spot patterns, which represent the crystal configuration in reciprocal space, were mainly used to obtain information about interplanar distances so-called d-spacings. This information can also be retrieved from Kikuchi patterns yet these were mainly used to accurately obtain orientations. The (mis)orientations were determined by a commercial TSL software package called A.C.T. 300.

2.4.3 Electron Dispersive Spectroscopy

The Energy Dispersive X-ray Spectroscopy (EDS) technique is based on the characteristic X-rays that are generated when an electron beam interacts with the specimen.

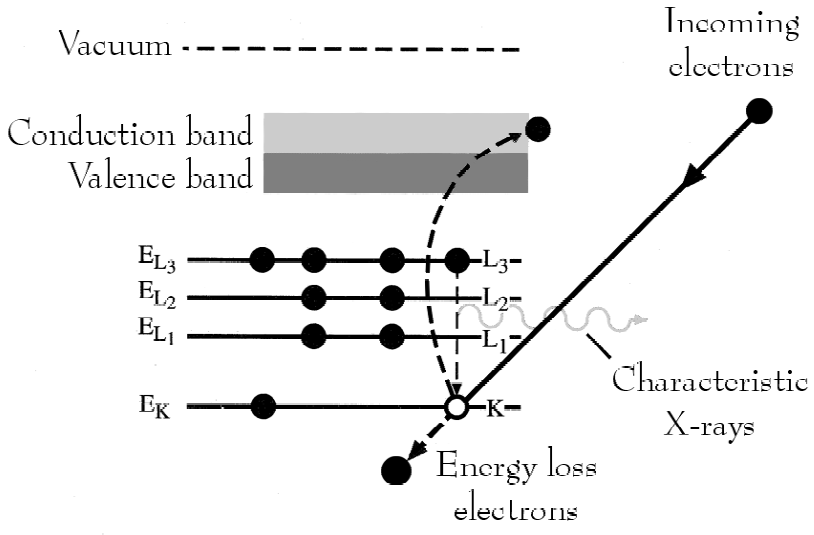

Fig. 2.16: Generation of characteristic X-rays.

The incident electrons may interact with the electrons within matter, present in for instance the K-shell of the atoms. The electron in this shell might be ejected, when a critical amount of energy is transferred, leaving the atom in an ionised state. The characteristic x-rays are generated as an electron out of the L or M shell fills this vacancy (Fig. 2.16). The energies between these shells are specific for each element. Therefore, capturing the energy of the characteristic X-rays allows identification of the illuminated element.

The characteristic X-rays produced, can be captured by the EDS detector within a discrete time interval. The number of counts should be sufficient to reach an acceptable signal to noise ratio. However, the time to acquire a spectrum should be tolerable to prevent possible sample drift, damage or contamination.

As a satisfactory spectrum is obtained, (Fig. 2.17) a quantification of the fraction of elements present in the illuminated area can be given. The peaks are extracted using a Gaussian deconvolution method after corrections have been performed on, for instance, escape peaks and background noise. The intensities of x-ray peaks are used to determine the relative concentrations of each element in the specimen making use of calibration files. This analytical method can be used as a powerful tool in phase determination.

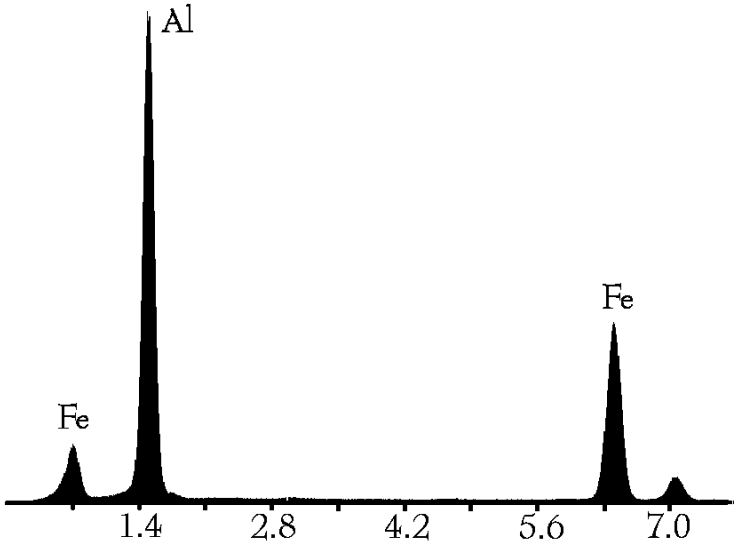

Fig. 2.17: Example of an EDS spectrum showing the röntgen peaks of Al and Fe (in keV).

2.5 Environmental Scanning Electron Microscope

The environmental scanning electron microscope (ESEM) retains all of the performance advantages of a conventional SEM, but removes the high vacuum constraint on the sample environment. It allows various settings through a range of pressures (as high as 10 Torr), temperatures (up to 1500°C) and several gas compositions. The advantage is that wet and non-conductive samples may be examined in their natural state without modification or preparation. In our case, the ESEM is used in combination with a tensile stage with heating unit to perform tensile tests on ULC Steel (Ch.3).

The essential features in the ESEM, to reach relatively low vacuum conditions, are the integration of two closely spaced pressure limiting apertures (PLA's) into the final lens of the electron column [16]. The regions below, between and above the PLA's are separately pumped to provide a graduated vacuum from

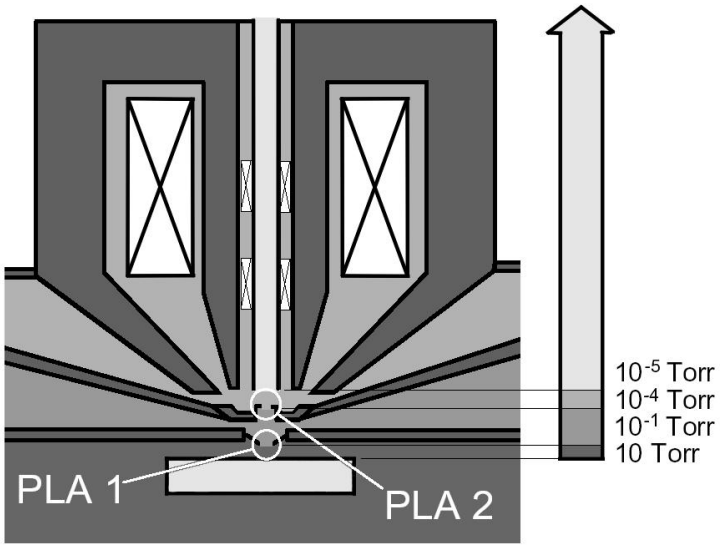

Fig. 2.18: Schematic representation of the ESEM pole piece including Pressure Limiting Apertures (PLA) and vacuum levels.

electron gun to sample chamber (Fig. 2.18). By locating the apertures close together at the bottom of the column, they reduce the distance the beam has to travel through the higher pressure stages. Therefore, most scattering of electrons that can affect resolution occurs between the final PLA and the sample surface, hence the need to reduce this distance to a minimum.

Unfortunately, the conventional Everhart-Thornley (ET) detector used in SEMs cannot function in these harsh chamber environments. The ESEM uses a gaseous environmental secondary detector (GESD) [17]. In its simplest form it is a conical electrode positioned apex down, concentric with the beam, at the bottom of the pole piece (Fig. 2.19). A positive potential of a few hundred volts, applied to the detector, attracts secondary electrons emitted by the sample. As the electrons accelerate in the detector field, they collide with gas molecules (for example H_2O, N_2, or mixtures). The resulting ionisations create additional electrons and positive ions. This process repeats many times resulting in a proportional cascade amplification of the original secondary electron signal.

The positive ions, generated by the signal amplification process, are attracted to the sample surface as charge accumulates. This minimises charging of the sample and allows observations on non-conducting samples.

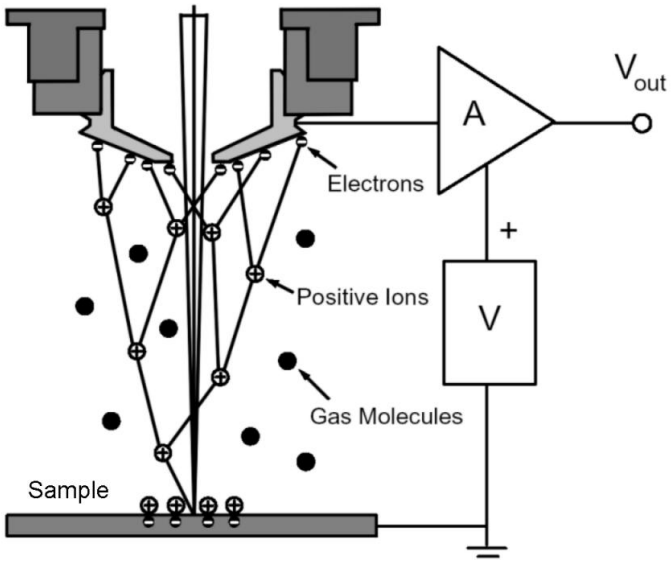

Fig. 2.19: Gaseous environmental secondary detector (GESD) cascade mechanism.

2.5.1 Tensile stage

The tensile stage used is a Kammrath & Weiss tensile module suited for the Philips XL 30 SEM. This substage can be fitted into the microscope chamber, which enables in-situ tensile testing. This allows dynamic surface deformation studies like slip band observations and crack initiation / propagation examinations.

The module can be fitted on the x-y table inside the microscope chamber (Fig. 2.20). This, however, disables the feature of sample motion in the z-direction. The electro-motor is placed parallel to the loading direction and may apply a force of 5000 N on the sample (Table 2.2). The framework of the substage is, however, constructed for a load of 10000 N. This will ensure maximum rigidity during performance, which is essential in the case of quantification of the data.

Table 2.2: Specifications of the tensile substage for the Philips XL 30 ESEM.

Max. Load	5000 N
Max. Displacement	10 mm
Displacement speed	0.2 to about 100 µm/s
Max. specimen thickness	4 mm
Max. specimen width	10 mm
Min. specimen length	38 mm
Max. specimen length	60 mm
Max. temperature	1000°C

As the clamps fix the sample, the load cell, which is configured at the back of the sample, may record the actual force acting on the sample during testing. This in combination with data on the elongation of the sample is of vital importance for a proper tensile test.

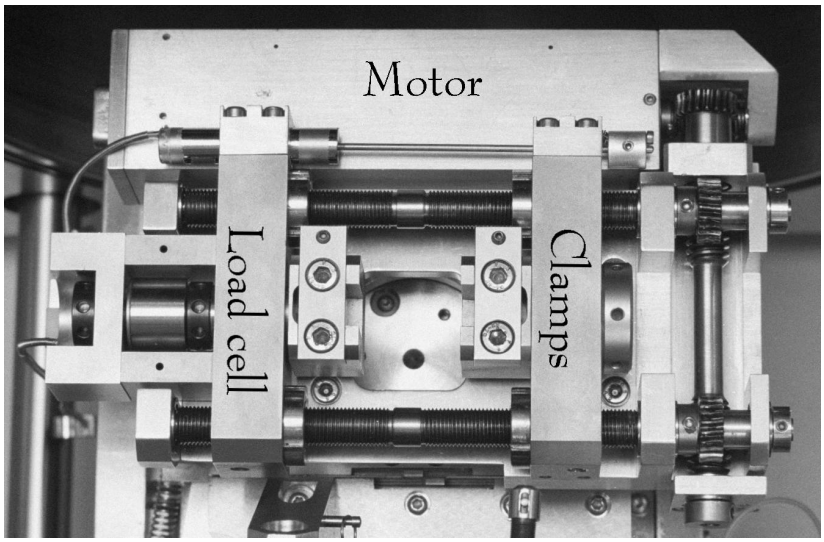

Fig. 2.20: Tensile sub-stage mounted on x-y table in Philips XL 30 ESEM.

References

1. J.I. Goldstein et al., Scanning electron microscopy and X-ray microanalysis, Plenum Press, New York, 1984.
2. H. E. Exner, Metals handbook, Metallography and microstructures, 89, vol. 9, 1985.
3. D.J. Dingley and V. Randle, Journal of materials science, vol. 27, 4545, 1992.
4. D.J. Dingley, Scanning electron microscopy, vol. 11, 569, 1984.
5. B.D. Cullity, Elements of X-ray diffraction, Addison-wesley, 1956.
6. A.J. Schwartz et al., Electron backscatter diffraction in materials science, Kluwer acadamic / Plenum publishers, 2000.
7. N.C. Krieger Lassen et al., Scanning microscopy, 115, vol. 6, 1992.
8. J. Illingworth and J. Kittler, Computer vision, vol. 44, 87, 1988.
9. D.P. Field, Ultramicroscopy, vol. 67, 1, 1997.
10. U.F. Kocks et al., Texture and Anisotropy: Preferred orientations in polycrystals and their effect on materials properties, Cambridge university press, 1998.
11. I. Samajdar and P. van Houtte, Mat. Sc. And Eng. A, vol. 238, 343, 1997.
12. I.L. Dillamore, Metallurgical reviews, vol. 10, 1965.
13. V. Randle, Acta Mater. , vol. 47, 4187, 1999.
14. D.G. Brandon, Acta Mater. , vol. 14, 1479, 1966.
15. S.I. Wright, PhD Thesis, Yale University, 1992.
16. G.D. Danilatos, Proc. 51st annual meeting of the microscopy society of America, 786, 1993.
17. K.R. Peeters, Proc. 50st annual meeting of the microscopy society of America, 1992.